Quantum Antidot Formation and Correlation to Optical Shift of Gold Nanoparticles Embedded in MgO

Jun Xu, J. Moxom, S. H. Overbury, and C. W. White
Oak Ridge National Laboratory, P.O. Box 2008, Oak Ridge, Tennessee 37831-6142

A. P. Mills, Jr.
Physics Department, University of California, Riverside, California 92521

R. Suzuki
Electrotechnical Laboratory, 1-1-4 Umezono, Tsukuba, Ibaraki 305, Japan
(Received 10 August 2001; published 16 April 2002)

Quantum antidots are subnanometer scale vacancy clusters, the localized electronic structure of which can significantly alter the properties of a nanomaterial. We use positron spectroscopy to study vacancy clusters generated during the formation of gold nanoparticles via ion implantation in an MgO matrix. We observed that quantum antidots are associated with the nanoparticle surfaces after annealing in an O_2 atmosphere, but not after annealing in a H_2 atmosphere. In the former case, the presence of quantum antidots bound to the gold nanoparticles correlates with the redshift of the gold surface plasmon resonance, thus allowing an explanation for the redshift based on the transfer of electrons away from the metal particles.

DOI: 10.1103/PhysRevLett.88.175502 PACS numbers: 61.72.Ji, 78.70.Bj

Quantum antidots are subnanometer scale vacancy clusters which have a localized electronic structure that can greatly affect the properties of nanomaterials by acting as localized repositories for electrons from the surrounding material. A great deal of literature has been accumulated on "antidot" or quantum void systems in semiconductor or metal-oxide thin films [1]. In this work we examine gold nanoparticles embedded in MgO that are of importance because of their unique optical and electronic properties [2–4]. A long-standing goal is to produce a network of narrow size distributed metallic nanoparticles in an oxide matrix with minimized imperfections. Ion implantation and sequential annealing are being used as a means to achieve this goal [5]. Noticeably, the creation of vacancy clusters, namely *quantum antidots,* and their various combinations is often associated with the nanoparticle formation processes. Also unavoidably, these vacancy clusters are expected to interact with embedded nanoparticles and alter the properties of nanosystems. It is of clear interest to detect these vacancy clusters, to investigate their origin, and to understand the effects of these voided clusters on material properties. We previously studied vacancy clusters generated during annealing of Au implanted MgO in an oxygen atmosphere [6]. In the present work, we find that the vacancy structure generated during annealing of the implanted MgO in a hydrogen atmosphere appears very different from the case of O_2 annealing.

Recently, it has been reported that the surface plasmon resonance wavelength of Au nanoparticles embedded in magnesia is shifted from 524 nm, which results from annealing in a H_2 atmosphere, to 560 nm when the nanoparticles are generated by annealing in an O_2 atmosphere [7]. The mechanism for such a shift has been unknown. In this paper we report our discovery that the "redshift" is correlated with the positron detection of vacancy clusters on the nanoparticle surfaces. A plausible explanation for the redshift is therefore that electrons are transferred from the nanoparticles to the vacancy clusters, leading to a decrease of the electron density on the metallic nanoparticles and a concomitant decrease in the surface plasma resonance frequency. The absence of the redshift in samples annealed in H_2 suggests that the vacancy clusters are changed by annealing in H_2. The possibilities include (1) inhibition of electron transfer due to hydrogen decoration of the antidots or (2) reduction of the size, density, or location of the antidots due to the absence of oxygen.

MgO(100) single crystals were implanted with 1.1 MeV gold ions at doses of 6×10^{16} Au ions/cm^2 in the Oak Ridge National Laboratory Surface Modification and Characterization (SMAC) research facility. The depth profiles of gold concentration were measured by Rutherford backscattering spectroscopy (RBS), using 2.3 MeV α particles, which shows that the Au implants are primarily located in the range of 0.16–0.4 μm, while the MgO remains crystalline after implantation. The implanted MgO crystals were annealed at 1200 °C in an Ar + O_2 (5%) or Ar + H_2 (5%) atmosphere for 10 h. Cross-section tunneling electron microscopy (XTEM) of these samples shows that rectangular Au metal nanoparticles are distributed in a size range of 0.5–7 nm with a peak population at 1.2 nm. Whether a H_2 or O_2 annealing atmosphere is used makes no difference in the XTEM images [8], although a "redshift" in the surface plasmon wavelength was observed for O_2 annealing [7].

Measurements of the Doppler broadening of positron annihilation photons were conducted using the ORNL

slow positron beam apparatus. The beam starts with a 20 mCi ^{22}Na source, which emits positrons with energies of a few hundred keV. Using a solid Ar moderator, fast positrons are converted into positrons of a few eV, which are then accelerated to energies varying from 300 eV–30 keV by applying a negative potential to the target. The normalized depth distribution of positrons is approximately $(x/\lambda^2)\exp\{-x^2/2\lambda^2\}$ and the mean positron penetration depth, $z = (\pi/2)^{1/2}\lambda$, is determined from the empirical relation $z\ [\mathrm{nm}] = (40/\rho)E^{1.6}$, where ρ is the density in g/cm^3 and E is the positron energy in keV [9]. Positron lifetime measurements were conducted using the positron beam line at the National Institute of Advanced Science and Technology. Positrons were produced by converting γ rays, generated by bombardment of a tantalum target with 75 MeV LINAC pulsed electrons, into electron-positron pairs that were then moderated in tungsten plates. The moderated positron pulses were stretched in a Penning trap and rebunched with a high frequency (178 MHz) and narrow width (<300 ps) [10].

The sizes of vacancy clusters were evaluated using beam-positron lifetime spectroscopy. The lifetime of positrons trapped in a vacancy cluster site is correlated to the size of the cluster. Figure 1 compares the positron lifetime spectra of 5 keV positrons injected into layers of Au nanoparticles formed by annealing at ~1200 °C for 10 h in Ar + 5% H_2 and with in Ar + 5% O_2. The implanted positron distribution has a mean penetration depth of 0.15 μm and a 40% overlap with the 0.16–0.4 μm Au nanoparticle region. Figure 1 also shows a lifetime spectrum for 23 keV positrons with a mean penetration depth of 1.7 μm, obtained from the O_2 annealed sample. This spectrum is used as a reference that is primarily characteristic of bulk MgO since in this case the overlap between the positron depth distribution and the implanted ion range is only about 3.4%. Note that both the MgO reference data and the data for O_2 annealing conditions were already reported in Ref. [6]. It is clearly seen that every spectrum shows fast and slow decays that depend on sample history. The fast decay of the H_2-annealed sample is close to that of the MgO reference, while its slow decay is close to that of the O_2-annealed sample.

The lifetime spectra were analyzed by Laplace inversion (CONTIN) [11], which deconvolutes the time spectra into the lifetime probability density function (pdf), as shown in the inset of Fig. 1. For the lifetime spectrum of the H_2 annealed sample, a fast lifetime component (0.22 ± 0.05) ns, which contributes (93 ± 3)% of events, is about the same as the MgO reference lifetime (0.22 ± 0.04). The slow lifetime component is (1.9 ± 0.4) ns at 7% contribution. For postimplantation O_2 annealing, the fast component is (0.41 ± 0.08) ns at 90% contribution, which was found to be due to clusters of four atomic vacancies, v_4, on the surface of nanoparticles [6]. The O_2 annealed sample does not exhibit a peak at 0.22 ns characteristic of trapping in the MgO reference layer, because all positrons are

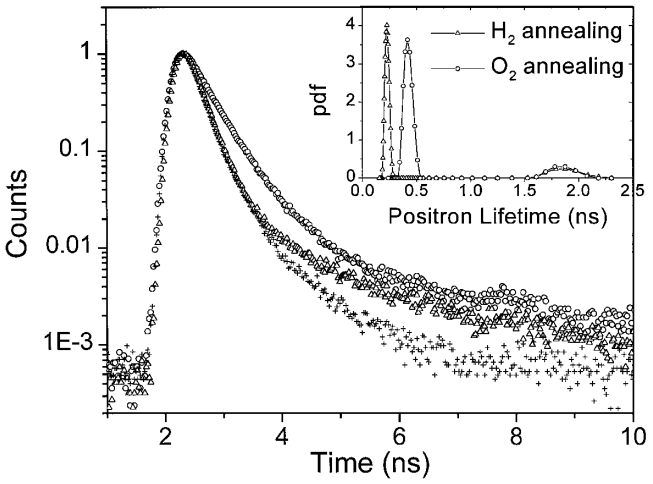

FIG. 1. Semilog plots of the counting rate as a function of the arrival time of annihilation γ rays for 5 keV positrons injecting into Au-implanted MgO annealed at ~1200 °C for 10 h in Ar + 5% O_2 atmosphere (circles) and in Ar + 5% H_2 atmosphere (triangles). A spectrum is also shown for 23 keV positrons on the O_2-annealed sample, characteristic of the bulk MgO. Inset: Probability density functions (pdf) as a function of positron lifetime, resulting from Laplace inversion (CONTIN) of lifetime spectra for Au nanoparticle layers generated in H_2 (triangles) and O_2 (circles) annealing atmospheres.

trapped at v_4 sites associated with the 0.41 ns lifetime. The slow component is (1.8 ± 0.3) ns at 7%, which is approximately the same as that for the H_2 annealed sample, and attributed to larger pores.

Depth profiles of vacancy clusters were evaluated by measuring the energy distribution of annihilation photons as a function of positron energy. The annihilation photo peak is centered at 511 keV, and broadened due to the Doppler effect induced by the electron momentum. Doppler broadening can be characterized by a shape parameter S, defined as the ratio of the counts appearing in the central region to the total counts in the annihilation photon peak [9]. The S parameter mainly represents the contribution from the vacancy concentration and size. Figure 2 shows the S parameter measured as a function of positron energy, corresponding to depth shown in the top scale, for MgO samples embedded with Au nanoparticles that were annealed at 1200 °C in Ar + 5% H_2 and Ar + 5% O_2, respectively. For O_2 annealing, the S parameter (open circles) is much larger than that of H_2 annealing. Therefore, the increased S parameter for O_2 annealing shows a higher vacancy concentration than that for H_2, which is consistent with the findings of positron lifetime measurements, i.e., excess vacancy clusters are found for O_2 annealing compared to H_2 annealing.

Types of defects in the unimplanted MgO samples include single vacancies, such as F centers and V centers, as shown by the 23 keV positron lifetime spectrum. During implantation, the major effect is formation of vacancies induced by high-energy collisions of Au with both Mg and

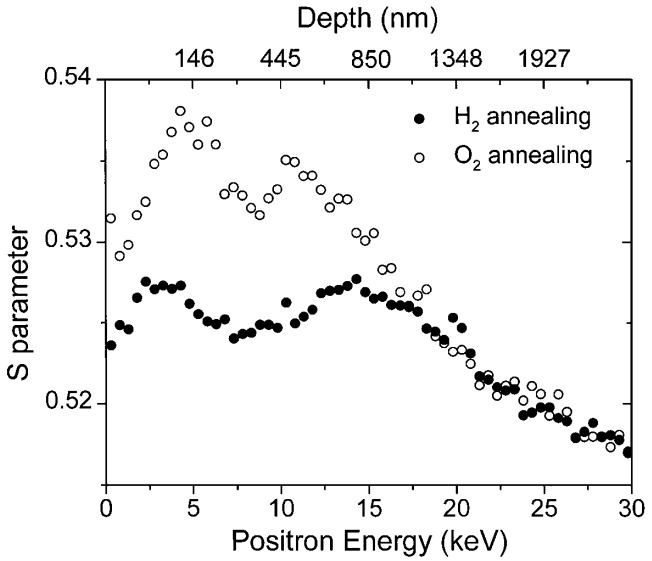

FIG. 2. S parameter as a function of positron energy for MgO samples that are Au ion implanted and annealed at ~1200 °C for 10 h in Ar + 5% H_2 (solid circles) and Ar + 5% O_2 (open circles), respectively.

O atoms, as well Au implants, vacancies, Mg, and O interstials in the bulk. As shown in previous work [6], vacancy defects after implantation before annealing are clustered as trivacancies and voids. The fate of these new constituents under annealing at a high temperature is expected to vary with exposure of the crystal to different annealing atmospheres.

During annealing in O_2, Au implants aggregate into crystallites and Mg and O vacancies can form v_4 vacancy clusters and larger voids. Our data show that these vacancy clusters may become attached to the Au nanoparticle surfaces, as evidenced by two-detector coincidence measurements of Doppler broadening of annihilation photons [6]. This also suggests that Au nanoparticles may play a role in forming the vacancy clusters. If the implanted MgO sample is annealed in H_2, v_4 clusters for the case of O_2 annealing and the trivacancy clusters for case before annealing were not found. It is possible that this effect is associated with H_2 diffusion into the bulk MgO or with lack of O_2 penetration.

The presence of vacancy clusters, which are observed after annealing in O_2, is correlated to the 26 nm redshift [7] of the 524 nm surface plasmon resonance frequency associated with the Au nanoparticles. This correlation between the observation of vacancy clusters by positrons and the "redshift" could be explained by the following mechanism. The redshift is caused by the transfer of electrons from the Au particles to localized states associated with the vacancy clusters, reducing the electron density, n, and thus the surface plasmon resonant frequency, $\omega_{sp} = (ne^2/\varepsilon_0 m)^{1/2}$, decreases accordingly, where e and m are the electron charge and the effective mass of the conduction electrons of Au particles, and ε_0 is the permittivity of vacuum. Indeed, a 6% decrease in the number of electrons on a colloid particle is all that would be needed to account the observed wavelength shift. If we assume that the peak-sized (1.2 nm) particles, which consist of 72 atoms per particle, make the greatest contribution to the shift, about 4 electrons transferred to nearby vacancy clusters would produce the observed shift. The effect of the H_2 annealing might be that the vacancy clusters are not formed at the Au nanoparticles, or that the vacancy clusters are changed due to the presence of H_2. In the latter instance, one possibility is that the clusters become decorated with hydrogen, thus eliminating their ability to accept electrons from the Au and simultaneously eliminating the attractive potential for positrons that causes the clusters to be visible in our experiments.

Electronic transfer from Au nanoparticles to vacancy clusters depends on the relative positions of the highest occupied orbital (HOMO) of the metallic nanoparticles and the localized states of the vacancy clusters. Figure 3 schematically shows the density of states diagram for the interface between a metallic nanoparticle and the MgO matrix in the presence of vacancy clusters. The bottom of the MgO conduction band is 1.3 eV below the vacuum level with a 7.8 eV gap to the top of valance band [12]. The partially occupied $6sp$ orbital of Au metal is 4.6 eV below the vacuum level and the fully occupied band of $5d$ electrons is 6.3 eV below the vacuum level [13]. If Au is present as nanoparticles, these energy levels are found by photoemission spectroscopy to depend on the size of the particle [14]. For 1.2 nm Au cubic particles, the $6sp$ electron energy is shifted by 0.9 eV toward the vacuum level and the $5d$ electrons shift 0.4 eV similarly. For electron transfer from the Au particles to the v_4 clusters, our data suggest that the v_4 localized state should be 2.6 eV higher than that of an F center, an oxygen vacancy occupied by two

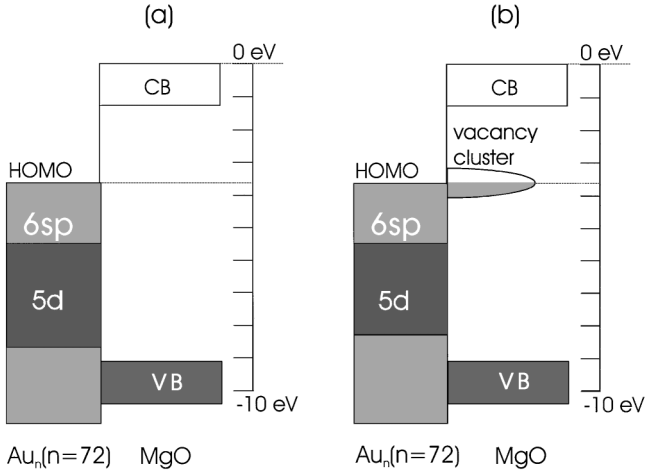

FIG. 3. Schematic diagrams of the energy band structure for the interface between Au nanoparticles and solid MgO. (a) Au nanoparticle with no surface defects. (b) Au nanoparticle with a surface vacancy cluster.

electrons. This suggestion is qualitatively consistent with an early finding that F_n centers produce an energy level higher than that of F centers [15]. The theoretical calculation from the well-known Mie theory [16] predicts that the surface resonance frequency is almost independent of the diameter of Au nanoparticles in nanometer range. This calculation may need to consider electronic unoccupied states of the nearby vacancy clusters for electron transfer.

In conclusion, we find that MgO samples containing Au nanoparticles annealed in H_2 exhibit neither a positron signal indicative of the presence of vacancy clusters, nor a plasmon resonance frequency shift. This strongly points to electron transfer from the nanoparticles to the vacancies as being the cause of the frequency shift. However, further measurements and more theoretical calculations are needed to evaluate whether the voids are absent when the shift is absent, or whether the voids are simply not observed by positrons when they are decorated by hydrogen, and not subject to electron transfer from the nanoparticles. A study of samples annealed in pure Ar might reveal the answer.

The authors would like to thank A. Ueda and D. Henderson of Fisk University for their contributions of samples. This research was sponsored by the Division of Chemical Sciences, Geosciences, and Biosciences, Office of Basic Energy Sciences, U.S. Department of Energy, under Contract No. DE-AC05-00OR22725 with Oak Ridge National Laboratory, managed and operated by UT-Battelle, LLC.

[1] I. J. Maasilta and V. J. Goldman, Phys. Rev. Lett. **84**, 1776 (2000), and references therein.

[2] J. D. Budai, C. W. White, S. P. Withrow, M. F. Chisholm, J. Zhu, and R. A. Zuhr, Nature (London) **390**, 384 (1997).

[3] W. C. W. Chan and S. Nie, Science **281**, 2016 (1998).

[4] S. Chen, R. S. Ingram, M. J. Hostetler, J. J. Pietron, R. W. Murray, T. G. Schaff, J. T. Khoury, M. M. Avarez, and R. L. Whetten, Science **280**, 2098 (1998).

[5] C. W. White *et al.,* Mater. Sci. Rep. **4**, 43 (1989).

[6] Jun Xu, A. P. Mills, Jr., A. Ueda, D. Henderson, R. Suzuki, and S. Ishibashi, Phys. Rev. Lett. **83**, 4586 (1999); Jun Xu, J. Moxom, B. Somieski, C. W. White, A. P. Mills, Jr., R. Suzuki, S. Ishibashi, A. Ueda, and D. Henderson, *Positron Annihilation ICPA-12,* edited by W. Triftshauser, G. Kogel, and P. Sperr (Trans Tech Publications, Zuerich, 2000), p. 637.

[7] A. Ueda *et al.,* Mater. Sci. Forum **239–241**, 675 (1997).

[8] D. Henderson (private communication).

[9] P. Asoka-Kumar, K. G. Lynn, and D. O. Welch, J. Appl. Phys. **76**, 4935 (1994).

[10] R. Suzuki, Y. Kobayashi, T. Mikado, H. Ohgaki, M. Chiwaki, and T. Yamazaki, in *Slow Positron Beam Techniques for Solids and Surfaces,* edited by E. Ottewitte and A. H. Weiss, AIP Conf. Proc. No. 303 (AIP, New York, 1994), p. 526.

[11] R. B. Gregory, Nucl. Instrum. Methods Phys. Res., Sect. A **302**, 496 (1991).

[12] L. H. Tjeng, A. R. Vos, and G. A. Sawatzky, Surf. Sci. **235**, 269 (1990).

[13] W. DeHeer, Rev. Mod. Phys. **65**, 611 (1993).

[14] K. J. Taylor, C. L. Pettiette-Hall, O. Cheshnovsky, and R. E. Smalley, J. Chem. Phys. **96**, 3319 (1992).

[15] B. D. Evans, J. Comas, and P. R. Malmberg, Phys. Rev. B **6**, 2453 (1972).

[16] C. F. Bohren and D. R. Huffman, *Absorption and Scattering of Light by Small Particles* (John Wiley & Sons, New York, 1983).